Cu-Nb Conductors Under Cyclic Loading

K. Han, V. J. Toplosky, Robert Goddard, Charles Swenson, Doan Ngoc Nguyen, *Member, IEEE*, and Victor Pantsyrny

***Abstract*—Pulsed magnets in the US National High Magnetic Field Laboratory (MagLab) use rectangular cross-section Cu matrix composite conductors. The strongest of these conductors incorporate various combinations of Cu reinforced by Nb-fibers. The slip systems of Cu and Nb are markedly incompatible during deformation because Cu has a face-centered cubic structure while Nb has a body-centered cubic structure. In order to reach the level of strength that we required in our conductors, Cu-Nb was subjected to especially high levels of deformation strain. This high strain level, in combination with the aforementioned incompatibility of deformation systems, resulted in very high internal stress within both Cu and Nb that greatly affected the future deformation behavior of the resulting Cu-Nb conductors, as reflected in the stress-strain curves generated by our tests, particularly the cyclic loading tests. At cryogenic temperatures, the thermal expansion difference between Nb fibers and Cu matrix added additional internal stress in the resulting conductors. We studied the mechanical deformation behavior of Nb-fiber-strengthened Cu under cyclic loading, and we examined the relationship between the microstructure of these conductors and their deformation behavior.**

***Index Terms*—Conductor, high strength, high conductivity, Young's modulus, mechanical strength.**

I. Introduction

RESEARCH at the National High Magnetic Field Laboratory (MagLab) has long been directed toward the development of a continuous supply of conductors for the 100T non-destructive pulsed magnet. The conductor used in the innermost coil (the "insert") of this magnet is the one that undergoes the highest stress level during operation [1], [2], [3]. Because its strength must exceed 1000 MPa, that conductor must be made of nanostructured composites [4], [5]. Researchers have used several methods for the manufacture of these composites, including Additive Manufacture (AM) [6] and Severe Plastic Deformation (SPD) [2], [7], [8], [9], [10]. Of these two methods, SPD has produced the highest mechanical strength in Cu-Nb [11], [12], [13]. SPD can be done by several methods, including repetitive roll-bonding, restacking, high-pressure torsion, or wiredrawing [14], [15], [16], [17], [18]. For this study, a combination of wiredrawing and restacking was chosen [4], [8], [9].

The process of extrusion is an important step in the preparation of a precursor material for wiredrawing. Extrusion can be either direct [19], [20], [21] or what is known as Equal-Channel Angular Extrusion (ECAE) [17]. Because excessive defects may be introduced by ECAE, direct extrusion was used instead [22], [23], [24], [25].

The strain introduced by the process of extrusion and drawing significantly exceeded the elastic deformation strain of the conductors. Consequently, significant plastic deformation occurred [26]. The later operation of the constructed magnet introduced further plastic deformation.

Plastic deformation can have at least three significant effects on magnet construction and magnet performance. First, large plastic deformation strain may cause changes in the cross-section area and in the overall shape of the conductor, decreasing the size of the cross-section area and consequently reducing the conductor's load-carrying capacity [2], [26]. Second, if the level of applied strain is near that of the homogeneous deformation strain in tensile tests, premature failure of the conductor may occur [27], [28], [29]. Third, because the Nb-strengthening fibres have a different crystal structure from that of the Cu matrix, high levels of internal stress will be introduced by SPD [30].

In our high-strength conductors, second phase fibres coexisted with the Cu matrix. A lattice misfit between the matrix and the particles will generate shortwave internal stresses [31], [32], [33]. Deformation alters these internal stresses so that longwave internal stresses are introduced as well as the shortwave ones. Longwave internal stresses may have a significant shear component, indicated by the presence of a shear microstructure [34], [35], [36], [37], [38], [39], [40], [41], [42]. This shear structure may affect not only tensile strength and conductivity, but also cyclic properties [10]. We performed experiments to clarify these property changes.

II. Experimental Methods

A. Materials

Our Cu–Nb conductors were fabricated by casting, forging, restacking, extruding, and cold drawing [8]. These conductors had nominal rectangular dimensions of 3.0×5.8 mm^2 with a 0.6 mm corner radius (corresponding to a cross-sectional area of 17.1 mm^2). This study was focused on samples from two spools: Spool 1 and Spool 3.

B. Mechanical Tests

Samples were machined with the tensile axis parallel to the longitudinal direction. Full- and reduced x-sectioned samples were tested at either room temperature (295 K) or liquid nitrogen

Received 25 July 2025; revised 11 October 2025; accepted 17 October 2025. Date of publication 7 November 2025; date of current version 2 January 2026. This work was supported in part by the National Science Foundation under Cooperative Agreement Number DMR-1644779 and DMR-2128556 performed at the National High Magnetic Field Laboratory (MagLab), and in part the State of Florida. *(Corresponding author: K. Han.)*

K. Han, V. J. Toplosky, and Robert Goddard are with the National High Magnetic Field Laboratory, Tallahassee, FL 32301 USA (e-mail: han@magnet.fsu.edu).

Charles Swenson is with the Lawrence Berkeley National Laboratory, Berkeley, CA 94720-8203 USA (e-mail: caswenson@lbl.gov).

Victor Pantsyrny is with the LLC Rosatom MetalTech, 115230 Moscow, Russia (e-mail: pantsyrny@gmail.com).

Doan Ngoc Nguyen is with the Los Alamos National Laboratory, Los Alamos, NM 87545, U.S.

Color versions of one or more figures in this article are available at https://doi.org/10.1109/TASC.2025.3630109.

Digital Object Identifier 10.1109/TASC.2025.3630109

temperature (77 K). Tensile tests were performed according to the guidelines given in ASTM-E8. These tests were conducted on a 100 kN capacity servo-hydraulic MTS machine with a controlled stroke rate of 0.5 mm/min. The machine was equipped with a cryostat. A clip-on axial extensometer with a 25 mm gauge-length was used to measure the strain in our tensile tests.

Our previous tests indicated that the properties of certain conductors can be changed by undergoing the process of either loading or unloading. To study the effects of loading cycles on various properties and to accurately measure the modulus of elasticity, we instructed our program to start the unload/reload cycle only after the observed onset of plastic strain (typically 1.5 to 2.0% strain) and then to load the specimen further until failure in stroke-control mode. We also conducted load-controlled cyclic tests according to guidelines in ASTM E466 and ASTM E606 at 77 K with a sinusoidal waveform (frequency = 5 to 10 hz). A diametrical extensometer was used to measure the strain in our cyclic tests.

C. Microstructure Examinations

Microstructure was investigated using either a Laser Scanning Confocal Microscope or a Zeiss 1540XB Field Emission Gun Scanning Electron Microscope (SEM). Most of the SEM images were taken at an accelerating voltage of 15 kV. We used an Energy Dispersion X-ray (EDX) spectrometer attached to the SEM for chemistry examinations.

III. Results

A. Microstructure

We examined microstructure in samples from Spool 1 and Spool 3. All samples had cladding with thickness less than 0.5 mm. The presence, inside this cladding, of Cu-Nb sub-elements with various shapes indicated that SPD had occurred during the shaping of the conductors from round to rectangular (Fig. 1). Most of the sub-elements near the Cu cladding on the narrow side of the conductor retained their original hexagonal shape. On the wider side of the conductor, however, the shape of most of the sub-elements shifted significantly as high levels of compressive and shear stress were applied during processing. These shape changes, in some samples, were significantly more severe at the center than at the edges.

The deformation of our wire included shear components that led to significant changes in the shape of the Cu-Nb sub-elements with the shear appearing more severe in some of the conductors than in others (Fig. 1).

In confocal microscopy images, we noticed grey scale changes within each Cu-Nb sub-element. Likewise, SEM images, particularly when taken by a back-scattered detector, showed similar grey scale changes, indicating variations in composition within each sub-element (Fig. 2).

EDS mapping revealed that Cu-Nb sub-elements were separated by pure Cu cladding. Within each sub-element, neither Cu nor Nb was uniformly distributed. Near the Cu cladding and at the centre of each sub-element, Nb content was lower than in other areas. Between these two Cu-rich regions, we observed several Cu-rich rings (Fig. 3). In longitudinal direction, the Nb showed a fiber shape. Researchers sometimes refer to this as ribbon shape because of the cross-section appearance.

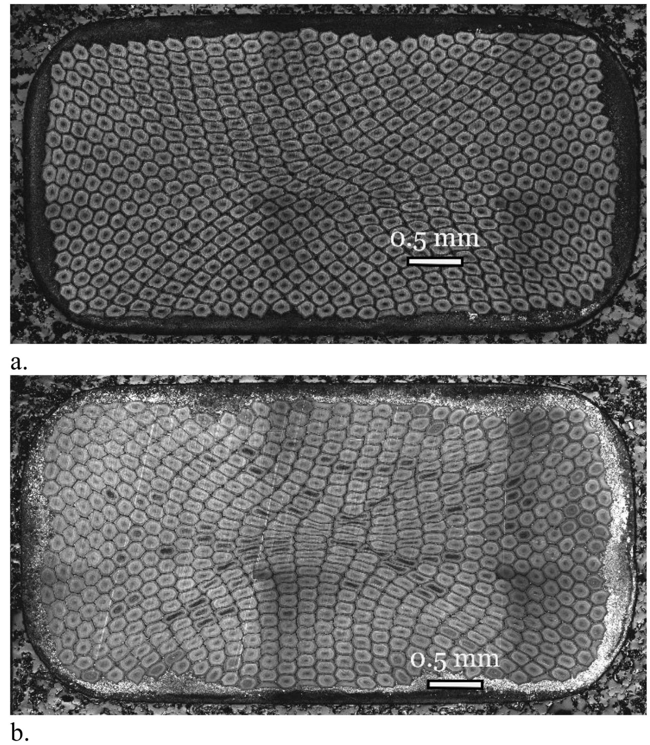

Fig. 1. Cross-section confocal microscopy images of Cu-Nb composite conductors. (a) An image from Spool 1. (b) An image from Spool 3. It appears that the center sub-elements of Spool 3 had deformed more than those of Spool 1, indicating that more shear deformation had occurred in Spool 3 than in Spool 1.

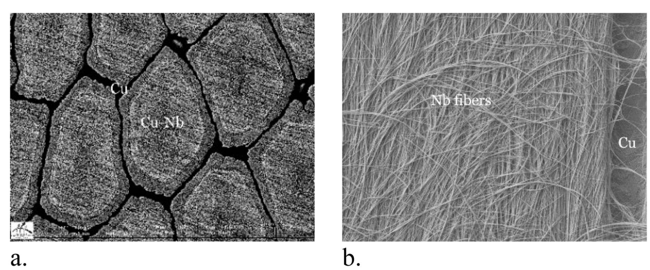

Fig. 2. SEM images of Cu-Nb composite samples from Spool 1. Thin Cu cladding is shown between the Cu-Nb sub-elements. Nb fibers and Cu-Nb are indicated in the figures. (a) X-section image; (b) Longitudinal image.

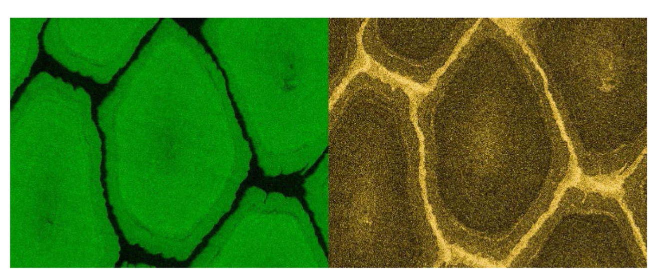

Fig. 3. EDS mapping of Nb (left panel) and Cu (right panel). Color intensity is proportional to the percentage of the elements measured.

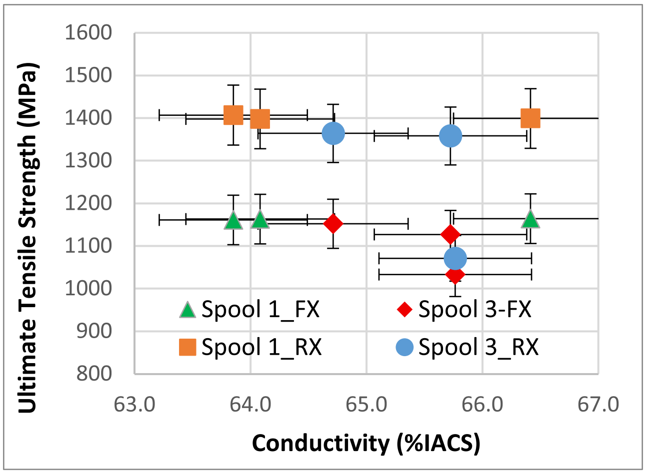

Fig. 4. Room temperature strength (UTS) vs conductivity of Spool 1 and Spool 3. FX = full x-section sample. RX = reduced x-section sample. Samples from Spool 1 show significantly less scattering in UTS data than those from Spool 3. The average value of UTS in Spool 1 is also higher. Error bars are the system error from our testing equipment.

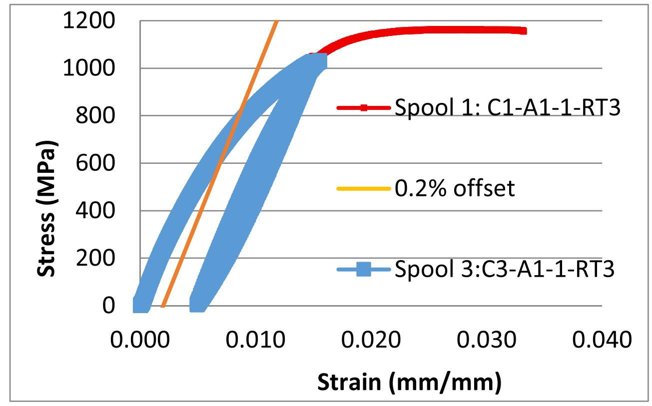

Fig. 5. Comparison of stress strain curves for Spool 1 (thin red line) and Spool 3 (thick blue line), tested at room temperature. 0.2% offset flow stress is identified by a straight line.

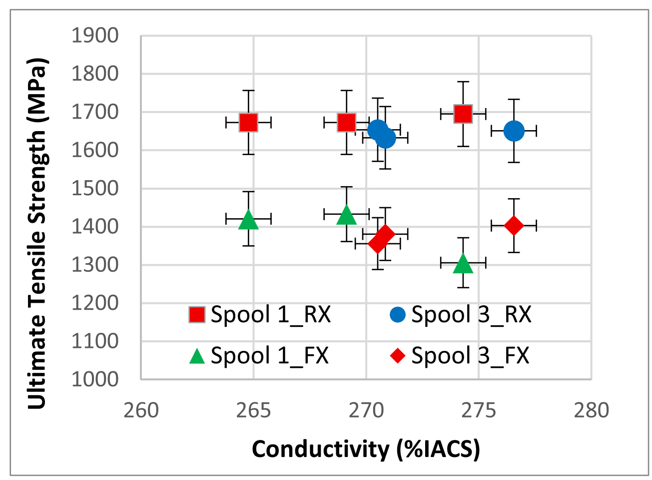

Fig. 6. 77 K strength (UTS) vs conductivity of Spool 1 and Spool 3. FX = full cross-section sample. RX = reduced cross-section sample. Samples from Spool 3 show less scattering than those from Spool 1 in UTS data. The average value of UTS for full cross-section samples in Spool 1 is almost identical to that of Spool 3. For reduced x-section samples, the average 0.2% offset flow stress and the UTS of Spool 1 are 1039 MPa and 1680 MPa, respectively, somewhat higher than those of Spool 3 (1023 MPa and 1642 MPa, respectively). Error bars are the system error from our testing equipment.

B. Mechanical Strength and Electrical Conductivity

On Spools 1 and 3, we performed tensile tests, which were designed to avoid any shear stress on samples. In these tests, we found marked differences between the samples taken from the two spools with respect to their mechanical strength at room temperature. The average Ultimate Tensile Strength (UTS) values of full x-section samples obtained at room temperature from Spool 1, for example, were higher than those obtained from Spool 3, leading us to assume the presence of more refined microstructure in Spool 1. At the same time, the UTS values from the Spool 1 samples were also less scattered, indicating that the microstructure was more homogeneous in samples from that spool.

Later, we again compared UTS values between Spool 1 and Spool 3 using reduced x-section samples rather than full x-section samples. After we removed part of the cladding from the conductors, we found that reduced x-section samples showed higher mechanical strength than full x-section samples, indicating that the Cu cladding had lower mechanical strength than the Cu-Nb. Spool 1 showed higher average UTS values and less scattered data than Spool 3 (Fig. 4).

Before fracture, full x-section samples from two spools showed almost identical stress-strain curves at room temperature (Fig. 5). Stress-strain curves in room temperature tests showed a high degree of rounding, indicating that large internal stresses had developed in samples from both spools. Beyond a strain level of 0.002 (0.2%) offset, all samples began to show a high degree of inelasticity, and the samples from Spool 3 progressed to Stage IV of plastic deformation: i.e., deformation with low strain hardening rate. One sample with a lower UTS failed even before Stage IV. We attributed this premature failure to the shear microstructure that had been developed in the materials during their fabrication. We concluded that the higher UTS values in the samples from Spool 1 resulted from the presence of a microstructure that was less shear rather than more refined microstructure.

All samples naturally showed higher strength at liquid nitrogen temperature (77 K) than at room temperature. The trend obtained in tests performed at 77 K closely followed that obtained in room temperature tests. The average UTS values for the reduced x-section samples obtained at 77 K from Spool 1 were higher than those from Spool 3 (Fig. 6). The average UTS values for cross-section samples obtained at 77 K from Spool 1 were almost identical to those from Spool 3. This indicates that the strength of Spool 3 samples was not intrinsically lower than that of Spool 1 samples. It is likely that, in our conductors, Spool 3 had more regions containing sheared sub-elements rather than sub-elements that had retained their original hexagonal shape.

At room temperatures, average conductivity values were almost identical for two spools. At 77 K, however, Spool 1 showed lower average conductivity values. In samples from Spool 1, we observed lower minimum electrical conductivity values and larger scattering in electrical conductivity.

C. Cyclic Loading

We performed our tests primarily under asymmetric tension–compression cyclic loads that had been designed to produce higher absolute values for tensile loading than for compression.

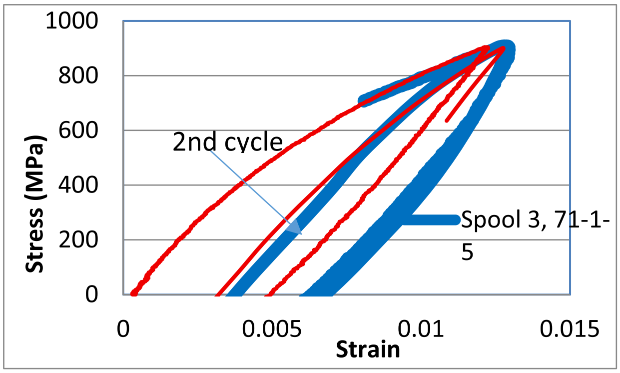

Fig. 7. Comparison of stress strain curves for samples from Spool 1 (thin red line) and Spool 3 (thick blue line), tested at 77 K under a maximum stress (σ_T) of ~910 MPa. The minimum stress levels for samples from Spools 1 and 3 are. 490 and 550 MPa, respectively. In the first cycle, plastic deformation strain amplitude values are approximately 0.5% and 0.6% for Spool 1 (sample 70-4-5) and Spool 3(sample 71-1-5), respectively. In the second cycle, plastic deformation strain amplitude values are approximately 0.12% and 0.18% for Spool 1 and Spool 3, respectively. A sample from Spool 1 survived 8388 cycles. A sample from Spool 3 survived 6319 cycles.

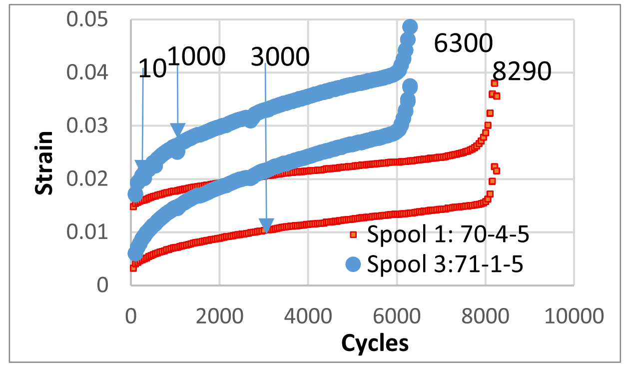

Fig. 8. Comparison of strain vs. number of cycles for samples from Spool 1 (thin red line) and Spool 3 (thick blue line) tested at under the same temperature and stress levels as the ones in Fig. 7. Both samples (70-4-5 and 71-1-5)) show increased strain with the number of cycles. The failure cycles are marked.

Throughout each series of tests, the relationship between tensile loads and compressive loads remained consistent from beginning to end. We tested each sample until failure, with most samples surviving more than 100 cycles. The highest levels of plastic deformation strain appeared in each sample during its first half-cycle.

Our tests were set at 77 K for a tensile stress (σ_T) of 910 MPa, ensuring that the σ_T level fell below the 0.2% offset flow stress levels of both spools: 1039 MPa for Spool 1 and 1023 MPa for Spool 3 obtained in tests of reduced x-section samples. Using dimetric strain measurements, we studied plastic deformation behavior under cyclic loading on samples from two spools. We found that the plastic deformation strain amplitude of Spool 1 at the end of the first half-cycle of loading was about 83% of that of Spool 3. At the end of the second full cycle of loading, the plastic deformation strain of Spool 1 was less than 70% of that of Spool 3 (Fig. 7). Our results demonstrated that, under the same tensile stress level used for cyclic tests, Spool 1 exhibited considerably less plastic deformation strain than Spool 3 at the same cycle.

We measured the strain levels when samples reached at either maximum or minimum stress levels. The data showed that the strain values increased rapidly during the first 1000 cycles and then increased at a lower rate. About 100 cycles before failure, strain values increased rapidly. The sample from Spool 1 lasted about 30% more cycles and failed at lower accumulated strain values than those of Spool 3 (Fig. 8).

IV. Discussion

The results of the tensile tests of the full x-section samples were often compromised by the presence of stress concentration near the grips. To avoid that problem, we used dog-bone-shaped samples. Spool 1 showed higher mechanical strength than Spool 3 in tests undertaken at room temperature and at 77 K using reduced x-section samples. The results for reduced x-section samples overestimated the strength of these samples because fabrication procedures had removed part of the lower strength Cu cladding.

Cu-Nb full x-section samples with higher mechanical strength exhibited lower electrical conductivity at 77 K, indicating that interface distance between Nb and impurity in Cu affected properties. This relationship was not obvious in our other test results, indicating that properties had been affected by both designed microstructure parameters (like the volume fraction of the cladding) and undesirable microstructure features (like shear defects). We believe that the shear structure in our conductors caused large changes in mechanical properties but not in electrical conductivity.

Our cyclic tests were performed under a tensile mean stress. Ratchetting occurred in the direction of increasing tensile strain (Fig. 8). At any given cycle (e.g., cycle 1000), the sample from Spool 1 showed less increase in cyclic plastic strain and greater displacement of the mean strain to a higher tensile level. The sample Spool 3 was also exposed to higher compressive stress levels. These factors led to less accumulation of damage in Spool 1 than in Spool 3.

V. Conclusion

We studied two spools (Spool 1 and Spool 3) of high-strength fiber-reinforced composites that had been produced by means of severe plastic deformation. We noticed that any variation in Nb content, such as Nb-depleted or Cu-rich rings within each sub-element, did not play a major role in a variation in properties between our samples. We also observed the presence of shear microstructure, the result of severe plastic deformation. The degree of shear appeared to impact on the mechanical properties of our conductors. Spool 1, which showed less shear microstructure, generally showed higher mechanical strength and less deformation strain under cyclic loading.

Acknowledgment

The authors would like to thank Mary Tyler for editing.

REFERENCES

[1] H. J. Schneider-Muntau, K. Han, N. A. Bednar, C. A. Swenson, and R. Walsh, "Materials for 100 T monocoil magnets," *IEEE Trans. Appl. Supercond.*, vol. 14, no. 2, pp. 1153–1156, Jun. 2004.

[2] K. Han et al., "Bending behavior of high-strength conductor," *IEEE Trans. Appl. Supercond.*, vol. 26, no. 4, Jun. 2016, Art. no. 8400804.

[3] K. Han, Y. Xin, V. J. Toplosky, R. M. Niu, and J. Lu, "Mechanical properties of a Ni-Co-Cr-Mo alloy," *IEEE Trans. Appl. Supercond.*, vol. 35, no. 5, Aug. 2025, Art. no. 7800105.

[4] K. Han, V. J. Toplosky, R. Walsh, C. Swenson, B. Lesch, and V. I. Pantsyrnyi, "Properties of high strength Cu-Nb conductor for pulsed magnet applications," *IEEE Trans. Appl. Supercond.*, vol. 12, no. 1, pp. 1176–1180, Mar. 2002.

[5] C. A. Swenson et al., "Progress of the insert coil for the US-NHMFL 100T multi-shot pulse magnet," *Physica B-Condens. Matter*, vol. 346, pp. 561–565, 2004.

[6] S. P. Ye et al., "Heterostructure and multiple nano-phases achieve superior strength-ductility-conductivity synergy of laser additive manufacturing copper alloy," *Virtual Phys. Prototyping*, vol. 20, no. 1, 2025, Art. no. e2437467.

[7] K. Han et al., "Material issues in the 100 T non-destructive magnet," *IEEE Trans. Appl. Supercond.*, vol. 10, no. 1, pp. 1277–1280, Mar. 2000.

[8] K. Han et al., "The fabrication, properties and microstructure of Cu-Ag and Cu-Nb composite conductors," *Mater. Sci. Eng. Struct. Mater. Properties Microstruct. Process.*, vol. 267, no. 1, pp. 99–114, 1999.

[9] K. Han, et al., "Cold-deformed Cu-Ag and Cu-Nb composites," *Ultrafine Grained Mater*, vol. 3, p.

[10] K. Han et al., "Internal stresses in cold-deformed Cu-Ag and Cu-Nb wires," *Philos. Mag.*, vol. 84, no. 24, pp. 2579–2593, 2004.

[11] W. A. Spitzig, "Strengthening in heavily deformation processed Cu-20% Nb," *Acta Metallurgica Et Materialia*, vol. 39, no. 6, pp. 1085–1090, 1991.

[12] J. D. Verhoeven et al., "Measurement of filament spacing in deformation processed Cu-Nb alloys," *Acta Metallurgica Et Materialia*, vol. 39, no. 11, pp. 2825–2834, 1991.

[13] W. A. Spitzig et al., "Effect of temperature on the strength and conductivity of a deformation processed Cu-20% -Fe composite," *J. Mater. Sci.*, vol. 27, no. 8, pp. 2005–2011, 1992.

[14] W. A. Spitzig, S. T. Kim, and P. M. Berge, "Development of low concentration deformation processed Cu-Nb And Cu-Cr alloys," *Mater. Manuf. Processes*, vol. 10, no. 3, pp. 353–371, 1995.

[15] F. Heringhaus and D. Raabe, "Recent advances in the manufacturing of copper-base composites," *J. Mater. Process. Technol.*, vol. 59, no. 4, pp. 367–372, 1996.

[16] V. I. Pantsymyi et al., "Development of Cu-Nb alloy microcomposite conductors for high field pulsed magnets," *IEEE Trans. Magn.*, vol. 32, no. 4, pp. 2866–2869, Jul. 1996.

[17] T. S. E. Summers et al., "ECAE-processed Cu-Nb and Cu-Ag nanocomposite wires for pulse magnet applications," *Adv. Cryogenic Eng. Mater.. Adv.*, vol. 42, pp. 499–505, 1996.

[18] D. Mattissen and D. Raabe, "Metallurgical production and cold deformation of a copper-niobium-silver in situ composite," *Metall*, vol. 51, no. 9, pp. 464–469, 1997.

[19] M. J. Demkowicz and L. Thilly, "Structure, shear resistance and interaction with point defects of interfaces in Cu-Nb nanocomposites synthesized by severe plastic deformation," *Acta Materialia*, vol. 59, no. 20, pp. 7744–7756, 2011.

[20] E. N. Popova et al., "Microstructural features in multicore Cu–Nb composites," *Materials*, vol. 14, no. 22, 2021, Art. no. 7033.

[21] I. L. Deryagina, E. N. Popova, and E. I. Patrakov, "Structure and properties of high-strength Cu-7.7 Nb composite wires under various steps of strain and annealing modes," *Metals*, vol. 13, no. 9, 2023, Art. no. 1576.

[22] V. Pantsyrny et al., "Stability aspects of the high strength high conductivity microcomposite Cu-Nb wires properties," *IEEE Trans. Appl. Supercond.*, vol. 16, no. 2, pp. 1656–1659, Jun. 2006.

[23] E. N. Popova et al., "Effect of deformation, annealing and doping with Zr on Nb filaments nanocrystalline structure in high-strength in situ Cu-Nb composites," in *Diffusion in Solids and Liquids: Mass Diffusion*, A. Ochsner and J. Gracio, Ed., Baech, Switzerland: Trans Tech Publications Ltd, 2006, pp. 299–304.

[24] M. J. R. Sandim, H. R. Z. Sandim, D. Stamopoulos, R. A. Renzetti, M. G. Das Virgens, and L. Ghivelder, "Spheroidization effects on the electrical and magnetic properties of Cu-Nb composites," *IEEE Trans. Appl. Supercond.*, vol. 16, no. 2, pp. 1692–1695, Jun. 2006.

[25] M. J. R. Sandim et al., "Size effects on the magnetic properties of Cu-Nb nanofilamentary wires processed by severe plastic deformation," *Supercond. Sci. Technol.*, vol. 19, no. 12, pp. 1233–1239, 2006.

[26] R. E. Goddard, K. Han, and D. N. Nguyen, "Relative strain in Cu-Nb composite wound wire," *Microscience Microanalysis*, vol. 22, pp. 1992–1993, 2016.

[27] K. Han et al., "Comparison of cu strengthened by ionic bonded particles and Cu strengthened by metallic bonded particles," *Materials*, vol. 18, no. 11, 2025, Art. no. 2648.

[28] R. Niu and K. Han, "Notch tolerance of high-strength Cu-based nanocomposites," *Mater. Characterization*, vol. 227, 2025, Art. no. 115293.

[29] R. Niu and K. Han, "Effect of notch geometry on the plastic behavior of Cu-Ag composites," *IEEE Trans. Appl. Supercond.*, vol. 34, no. 5, Aug. 2024, Art. no. 6800305.

[30] K. Han, V. J. Toplosky, R. M. Niu, and J. Lu, "Internal stress in high-strength CuAg conductor," *IEEE Trans. Appl. Supercond.*, vol. 34, no. 5, Aug. 2024, Art. no. 7000105.

[31] A. Ishmaku and K. Han, "Characterization of cold-rolled Cu-Nb composite," in *Progress in Advanced Materials and Processes*, D.P. Uskokovic, S.K. Milonjic, and D.I. Rakovic, Ed., Baech, Switzerland: Trans Tech Publications Ltd, 2004, pp. 479–484.

[32] Y. Leprince-Wang et al., "Microstructure in Cu-Nb microcomposites," *Mater. Sci. Eng. Struct. Mater. Properties Microstructure Process.*, vol. 351, no. 1/2, pp. 214–223, 2003.

[33] K. Yu-Zhang et al., "Transmission electron microscopy investigation of the atomic structure of interfaces in nanoscale Cu-Nb multilayers," *Philos. Mag.*, vol. 88, no. 17, pp. 2559–2567, 2008.

[34] L. Deng et al., "Effects of interface area density and solid solution on the microhardness of Cu-Nb microcomposite wires," *Mater. Characterization*, vol. 150, pp. 62–66, 2019.

[35] L. Deng et al., "Response of microstructure to annealing in in situ Cu–Nb microcomposite," *J. Mater. Sci.*, vol. 54, no. 1, pp. 840–850, 2019.

[36] L. P. Deng et al., "Hardness, electrical resistivity, and modeling of in situ Cu-Nb microcomposites," *J. Alloys Compounds*, vol. 602, pp. 331–338, 2014.

[37] L. P. Deng et al., "Thermal stability of Cu-Nb microcomposite wires," *Acta Materialia*, vol. 101, pp. 181–188, 2015.

[38] L. P. Deng et al., "Thermal stability of Cu-Nb microcomposite wires," *Acta Materialia*, vol. 101, pp. 519–519, 2015.

[39] L. P. Deng et al., "Effect of extra Cu on the strength and conductivity of Cu-Nb microcomposite wires," *Rare Metal Mater. Eng.*, vol. 44, no. 7, pp. 1696–1701, 2015.

[40] L. P. Deng et al., "Effect of annealing on the microstructure and properties of in-situ Cu-Nb microcomposite wires," *Acta Metallurgica Sinica-English Lett.*, vol. 29, no. 7, pp. 668–673, 2016.

[41] L. P. Deng et al., "Microstructure and texture evolution of Cu-Nb composite wires," *Mater. Characterization*, vol. 81, pp. 124–133, 2013.

[42] L. P. Deng et al., "Study on the microstructure evolution of Cu-Nb composite wires during deformation and annealing," *Acta Metallurgica Sinica*, vol. 50, no. 2, pp. 231–237, 2014.